Extreme Refractive Index Wing Scale Beads Containing Dense Pterin Pigments Cause the Bright Colors of Pierid Butterflies

Bodo D. Wilts, Bas Wijnen, Hein L. Leertouwer, Ullrich Steiner, and Doekele G. Stavenga*

Butterflies of the family Pieridae are brightly colored, ranging from white to red, caused by various pterin pigments concentrated in scattering spheroidal beads in the wing scales. Given the sparsity of the beads in the wing scales, the high brightness suggests a scattering strength of the beads that significantly surpasses that of typical cuticular chitin beads with the areal density found in the wing scales. To elucidate this apparent contradiction, the optical signature of the pierids' highly saturated pigmentary colors are analyzed by using Jamin–Lebedeff interference microscopy combined with Kramers–Kronig theory and light scattering modeling. This study shows that extreme pterin pigment concentrations cause a very high refractive index of the beads with values above 2 across the visible wavelength range, thus creating one of the most highly light scattering media thus far discovered in the animal kingdom.

1. Introduction

Brilliant colors rely on the efficient reflection of light either by scattering from pigment (or dye) containing materials or by light interference from periodic structures with features in the ≈100 nm range.[1,2] Both approaches require a high refractive index contrast, which is technologically implemented by the use of high refractive index materials, often metal oxides, carbides, or selenides.[3,4] The coloration in animals is, on the other hand, restricted to organic compounds with a limited range in refractive indices.[1,5,6] Nevertheless, both pigmentary and structural colors in nature often surpass artificially made counterparts in terms of brightness, color-purity, and materials' use.[7,8] Particularly, in certain butterfly species that rely on scattering of light from their wing scales, the unusual brightness in color arising from a scarce assembly of scatterers is baffling and the detailed explanation of the underlying phenomena is likely to lead to interesting new coloration technologies.

The universally enjoyed rich coloration of butterflies resides in a dense lattice of colored wing scales. The basic butterfly wing scale consists of a flat lower lamina that acts as the foundation for a regular-ordered array of parallel ridges, which are connected by more or less regular arranged cross-ribs.[9,10] When pigmented, the butterfly wing scales generally harbor their pigment in the ridges and cross-ribs. Butterflies of the family Pieridae are unique, however, as the wing scale cross-ribs serve as substrates for numerous amounts of rice-grain-shaped beads.[11] These granules contain various pterin pigments: leucopterin, xanthopterin, and/or erythropterin.[12] Leucopterin absorbs exclusively in the ultraviolet, resulting in a low reflectance of the wing scales in the ultraviolet (UV) and, because of the granular composition of the scales, in a high reflectance in the (for humans) visible wavelength range due to scattering of nonabsorbed light. Wing scales that carry beads filled with leucopterin therefore appear white. However, for the butterflies themselves, the wings are distinctly colored, because they have ultraviolet-sensitive photoreceptors in addition to blue-, green-, and red-sensitive photoreceptors.[13] Xanthopterin and erythropterin have distinct absorption bands in the violet-blue and blue-green wavelength ranges, respectively, causing yellow, orange, or red wing colors.[12,14]

Because of the pterins' short-wavelength absorption bands, the pigmented scale granules act as high-pass spectral filters. Outside their absorption bands, the beads act as strong scatterers because of their refractive index contrast with the surrounding air. In the butterfly world, a granular medium like the one observed in the pierid butterflies seems to be uniquely evolved; however, granular arrangements of pigmented matter are rather common in the animal kingdom. Similar photonic structures can, for example, be recognized in damselflies[15] and cuttlefish.[16,17] In the case of marine animals, the effective refractive index contrasts – and thus the additional scattering components – are less strong, due to the higher refractive index of the medium surrounding the granules (water, $n_w \approx 1.33$). A strong pigmentation still facilitates enhanced scattering, but

Dr. B. D. Wilts, Prof. U. Steiner
Adolphe Merkle Institute
University of Fribourg
Chemin des Verdiers 4, CH-1700 Fribourg, Switzerland
E-mail: bodo.wilts@unifr.ch
Dr. B. D. Wilts, Dr. B. Wijnen, H. L. Leertouwer, Prof. D. G. Stavenga
Computational Physics
Zernike Institute for Advanced Materials
University of Groningen
Nijenborgh 4, NL-9747AG Groningen, The Netherlands

DOI: 10.1002/adom.201600879

extreme effects can hence most likely only be realized by air-based granular media as those found in pierid wing scales.

The refractive index of the common butterfly wing material, chitin, is ≈1.56,[18,19] but the observed bright colors suggest an extreme scattering strength of the chitin beads in the pierid wing scales. We have therefore conducted a quantitative analysis of the pterin pigments contained in the scale beads of four differently colored pierid butterflies. To determine the refractive index of the wing scales, Jamin–Lebedeff interference microscopy was employed. Additional microspectrophotometry of isolated scales yielded a high absorbance, implying substantial contributions of the pigments to the refractive index spectrum. The two methods enable to establish the intimate connection between the measured refractive index dispersion and the absorption spectra using the Kramers–Kronig relation.[6]

2. Results

2.1. Pierid Butterflies Widely Differ in Wing Coloration

Previous work demonstrated that the wing coloration of pierid butterflies is due to various pterin pigments.[11,12,20] The aim of the present study is to assess the possible contribution of the pigments to the refractive index of the wing scales, in order to gain further insight into the optics of wing coloration. To investigate the effect of different pterin pigments, we studied the wings of males of four pierid butterfly species: the Small White, *Pieris rapae*, the Cloudless Sulphur, *Phoebis sennae*, the Orange Tip, *Anthocharis cardamines*, and the Common Jezebel, *Delias nigrina*. The wings of *P. rapae* have an almost homogeneous bright white color at both the upper (dorsal; **Figure 1**a) and lower (ventral) side; small black-brown areas break the monocolored pattern. Both sides of the wings of *P. sennae* are bright yellow (Figure 1b). The dorsal forewings of male *A. cardamines* have characteristic, bright orange-colored tips in addition to the main whitish color (Figure 1c; the ventral wings have a somewhat variegated patterning). In contrast, the dorsal wings of male *D. nigrina* are mainly white, with blackish tips, and the lower (ventral) wings are mainly brown-black, with yellow bands in the forewings and red bands in the hindwings (Figure 1d).

We focused our analysis on four differently colored wing areas: a white area of *P. rapae*, a yellow area of *P. sennae*, an orange tip area of *A. cardamines*, and a red band area of *D. nigrina*. Figure 1e presents reflectance spectra of the four wing areas measured with a bifurcated probe. All four spectra show the characteristic sigmoidal shape of pigmentary colored materials, with low (high) reflectance at short (long) wavelengths.

2.2. The Size of the Scale Beads is Species-Specific

The different wing colors are due to pterin pigments localized in small beads in the wing scales. We investigated the beads of the four colored wing areas by scanning electron microscopy (**Figure 2**a and Figure S1 (Supporting Information)). In all cases, the beads had an approximately prolate spheroid shape, seen in transmission electron micrographs (Figure 2b). The

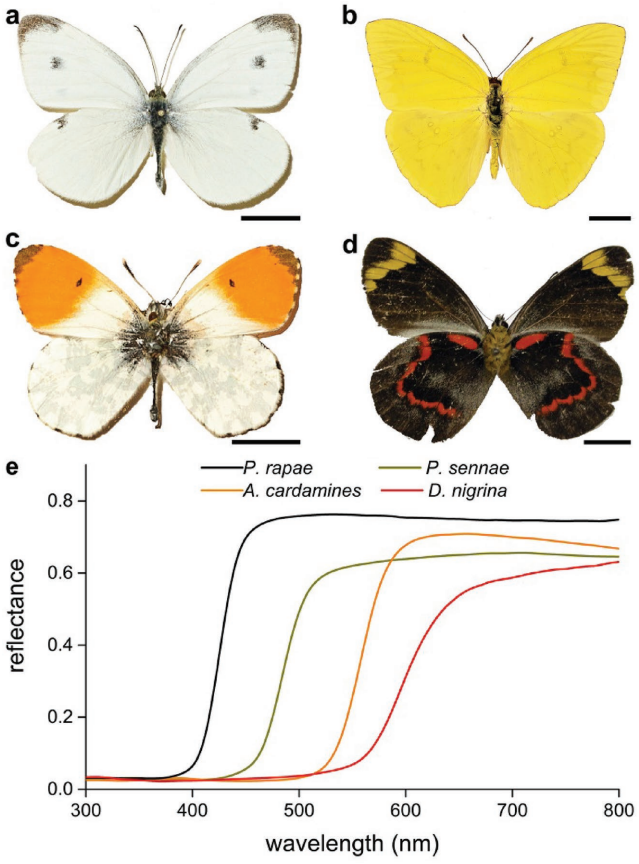

Figure 1. The investigated male pierid butterflies and wing reflectance spectra. a) The Small White, *Pieris rapae*. b) The Cloudless Sulphur, *Phoebis sennae*. c) The Orange Tip, *Anthocharis cardamines*. d) The Common Jezebel, *Delias nigrina* ((a–c) upper or dorsal wings, (d) lower or ventral wings). e) Reflectance spectra measured with a bifurcated probe of the white wing of *P. rapae*, the yellow wing of *P. sennae*, the orange tip of *A. anthocharis*, and a red band of *D. nigrina*. Scale bars in (a–d): 1 cm.

ellipsoidal beads are attached to the scale cross-ribs with the long axis of the spheroids perpendicular to the scale plane.

From the scanning electron micrographs, we estimated the length, l_b, and width, w_b, of the beads of the various scales (Figure 2c and **Table 1**). Those of the white scales of *P. rapae* were on average shortest, with a length $l_b \approx 450$ nm, compared to those of the yellow, orange, and red scales, which were 600–1100 nm long; the width, $w_b \approx 200$ nm was rather similar in the four species (Figure 2d).

In the scanning electron microscopy (SEM) images, the set of beads of the scales form a monolayer, which is not completely continuous due to the voids in-between the granules. To estimate the volume-fraction f_V taken up by the beads, we estimated the cross-sectional area filling fraction f_A of the beads from top-view SEM images (Table 1), because the beads are very approximately arranged along the long axis of the bead. The cross-sectional area of a bead in top-view is $A_b = \pi w_b^2/4$, or, the volume of a cylinder with cross-section A_b and length l_b is $\pi w_b^2 l_b/4$. The volume of a single spheroid is $\pi w_b^2 l_b/6$, giving rise to a bead volume filling factor of a layer with thickness l_b of $f_V = 2f_A/3$ (vide infra).

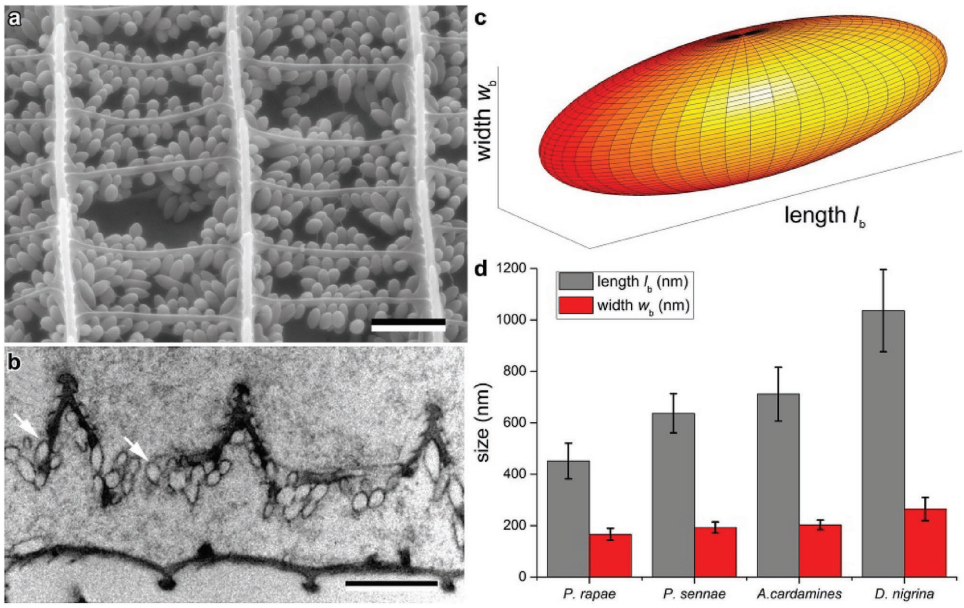

Figure 2. Anatomy of a *P. rapae* wing scale and scale bead dimensions. a) Scanning electron micrograph showing numerous ellipsoidal beads attached to the cross-ribs and ridges (scale bar: 1 µm; adapted from ref. [11]). b) Transmission electron micrograph of a wing scale of *P. rapae* (scale bar: 1 µm). c) Diagram of a wing scale bead as a prolate spheroid. d) The length and width of the beads of the four butterfly species as determined from scanning electron micrographs (see also Table 1).

2.3. Refractive Index of Pierid Butterfly Wing Scales

The refractive index contrast of the beads with air causes the bright colors of the pierid wings. We measured the refractive index of the wing scales as a function of wavelength using the recently developed Jamin–Lebedeff interference microscopy method.[6,18,21] In short, Jamin–Lebedeff interference microscopy determines the refractive index of a material by immersing it in various refractive index fluids and measuring the resulting phase shift as a function of wavelength. The zero-intercept of linear fits to these phase retardations as a function of the refractive indices of the surrounding media yields the (real part of the) spectrally resolved refractive index of the medium of interest.[6,18,21] **Figure 3**a presents results for the four differently colored scale types together with the refractive index of chitin, the ingredient material of butterfly wing scales.[18] The refractive indices of the four butterfly scales appeared to be distinctly higher than that of chitin and showed a signature of anomalous dispersion that is characteristic for strongly absorbing media.[6] The Jamin–Lebedeff experiments yielded in addition the effective thickness d_s of the scales, for *P. rapae*, *P. sennae*, *A. cardamines*, and *D. nigrina* of 0.65, 0.90, 0.78, and 1.2 µm, respectively (Table 1). These thickness values are averages over large areas, including the upper lamina containing the pigmented beads and the chitinous ridges and cross-ribs and the lower lamina consisting of pure chitin. The thickness values are therefore effective thicknesses, determined from scales immersed in refractive index fluid. Not surprisingly, the estimated effective scale thicknesses closely match the bead lengths (Table 1).

Table 1. Scale thickness (d_s), bead length (l_b), bead width (w_b), aspect ratio of the beads, cross-sectional area filling fraction (f_A), and bead fraction (f_b).

Species	d_s [µm]	l_b [nm]	w_b [nm]	Aspect ratio	f_A	f_b
P. rapae	0.65	451 ± 69	166 ± 23	2.7 ± 0.2	0.47 ± 0.03	0.22 ± 0.03
P. sennae	0.90	637 ± 76	193 ± 22	3.3 ± 0.3	0.44 ± 0.02	0.20 ± 0.03
A. cardamines	0.78	711 ± 105	203 ± 19	3.5 ± 0.5	0.51 ± 0.04	0.30 ± 0.04
D. nigrina	1.2	1096 ± 160	274 ± 45	4.0 ± 0.8	0.32 ± 0.02	0.19 ± 0.03

2.4. Contribution of the Different Pterin Pigments to the Refractive Index

As the anomalous dispersion of the refractive indices is presumably caused by the pterin pigments in the scale beads, we assessed the scale absorbance spectra. We therefore measured the transmittance of the central area of single wing scales immersed in a refractive-index-matching fluid that inhibits interfacial scattering. As expected, the white, yellow, orange, and red scales absorbed strongly in the ultraviolet, violet, blue-green, and violet to orange wavelength ranges, respectively; the peak absorbance (A_{max}) was ≈0.8 (Figure S2 (Supporting Information) and **Table 2**).

Using the volume filling fractions of the bead layers (f_V) derived above, the effective absorption coefficient of the material was derived from the measured absorbance spectra (Experimental Section, Equation (1)), yielding peak values of 1–3 µm^{-1}. Figure 3b presents the associated imaginary part of the refractive index. Using the Kramers–Kronig dispersion relation (Experimental Section, Equation (2); see also refs. [22] and [23]), the contribution of the pigments to the (real part of the)

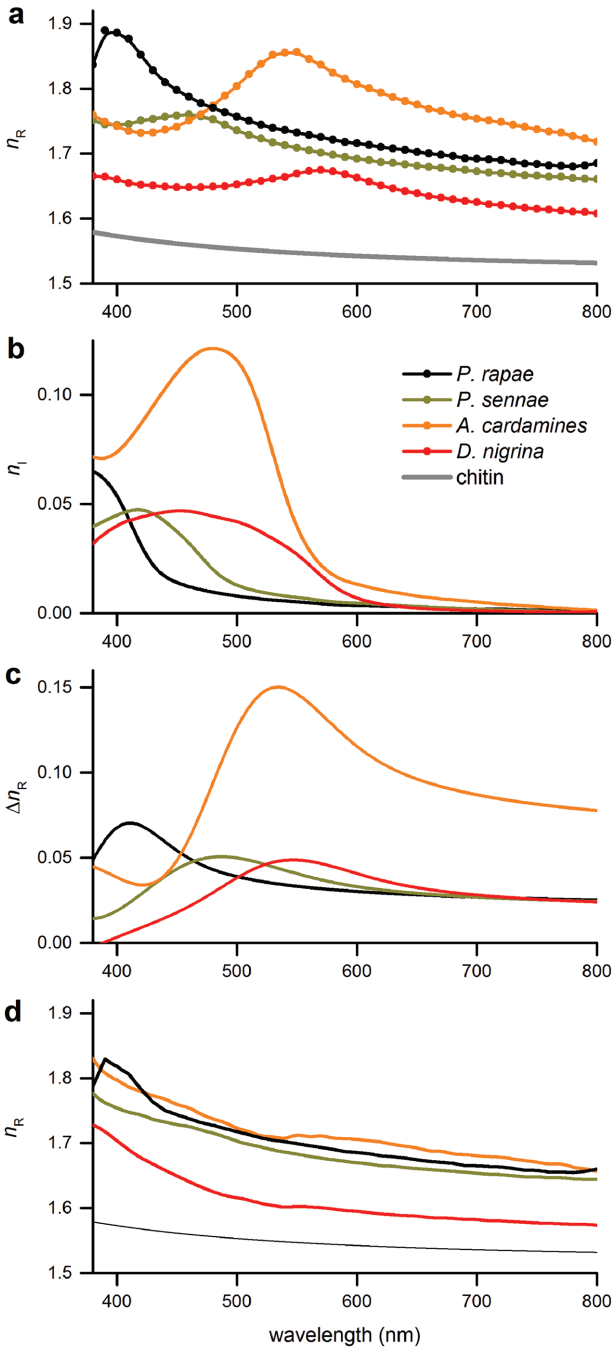

Figure 3. Refractive index spectra of wing scales of the four pierid butterflies. a) Real part of the refractive index spectra measured with Jamin–Lebedeff interference microscopy. For comparison, the refractive index of chitin, determined in unpigmented butterfly wing scales,[18] is added. b) Imaginary part of the refractive index derived from absorbance measurements (Figure S1, Supporting Information). c) The contribution of the pterin absorption to the real part of the refractive index according to the Kramers–Kronig dispersion relation. d) Wing scale refractive index spectra obtained by subtracting the calculated refractive index difference spectra of (c) from the measured spectra of (a).

refractive index $\Delta n_R(\lambda)$ was calculated (Figure 3c). The anomalous dispersion of the calculated spectra closely resembles the measured data of Figure 3a.

Table 2. Pigment, peak wavelength (λ_{max}), and peak absorbance (A_{max}) of the investigated butterfly beads.

Species	Main pigment	λ_{max} [nm]	A_{max}
P. rapae	Leucopterin	365	0.8
P. sennae	Xanthopterin	410	0.8
A. cardamines	Erythropterin	470	0.8
D. nigrina	Mixture	380–450	0.6

Subtracting the calculated $\Delta n_R(\lambda)$ of Figure 3b from the measured $n_R(\lambda)$ of Figure 3c yielded rather smooth spectra with approximately the dispersion of chitin (Figure 3d). The resulting refractive index spectra are all distinctly higher than that of chitin. The difference is due to very short-wavelength (far-UV and UV wavelengths <380 nm) absorption in pterins, causing normal dispersion, i.e., a decreasing refractive index with increasing wavelength, in the visible wavelength range.

2.5. Refractive Index of the Pigmented Beads

The derived refractive index spectra of intact scales arise from the combination of all optical components in the optical path. The scale's material components contributing to the measured refractive index are the pterins in the scale beads and chitin in the lower lamina, the ridges, and the cross-ribs. With bead and chitin refractive indices n_b and n_c, the measured refractive index is $n_s = f_b n_b + f_c n_c$, where f_b and $f_c = 1 - f_b$ are the fractional contributions of the two materials. The bead fraction $f_b = f_V l_b / d_s$ is obtained from the estimated bead layer thickness l_b, the scale thickness d_s, and the volume fraction of the beads in the bead layer f_V, yielding a refractive index of the beads of $n_b = n_c + (n_s - n_c)/f_b$ (**Figure 4**).

Note that a more advanced effective medium theory using Bruggeman's approach of ellipsoidal inclusions[22,24,25] produces virtually identical results (Figure S3, Supporting Information) due to the fact that our measurements were performed by embedding the butterfly scales in nearly refractive index

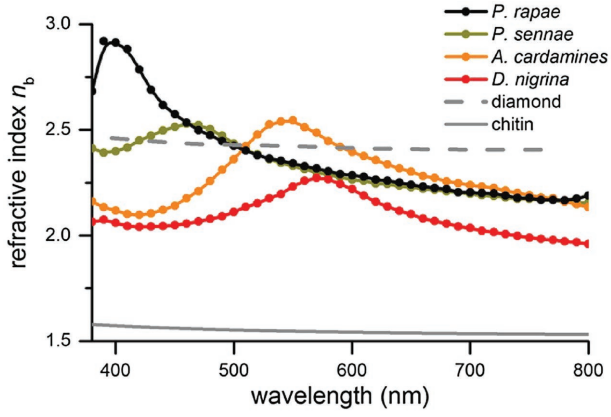

Figure 4. Refractive index of individual scale beads as a function of wavelength derived from Figure 3, using the bead filling factor assessed from scanning electron micrographs. The refractive index of scale chitin and diamond are added for comparison.

matching media, so that the differences in refractive indices of the various material components are small. In this limit, the essential optical parameters are the refractive index contrasts or differences, so that the various effective medium approximations are about equivalent to a simple weighting factor approach.

The resulting refractive index values of the beads (Figure 4 and Figure S2 (Supporting Information)) are well above 2 across the entire visible wavelength range, which is unusually high for biological matter (cf. the value for pure diamond: ≈2.42). When compared to pure chitin, the increase in refractive index with respect to air is almost twofold.

2.6. Mie Modeling

To estimate the scattering properties of the scale beads and to elucidate the effect of the unusually high refractive index values, we performed optical modeling. Analytical solutions for light scattering, so-called Mie or Lorentz–Mie solutions, only exist for spheres and cylinder geometries, and thus advanced modeling techniques are required for the spheroidal beads. We executed finite-difference time-domain simulations of the differently sized spheroids. In addition, we also studied analytic solutions of a dielectric sphere. **Figure 5**a shows the corresponding radial scattering plots.

The dielectric sphere scatters light as expected for a common dielectric: shorter wavelengths are scattered more strongly than longer wavelengths.[26,27] For the spheroids of the butterfly scale beads, light scattering differs; scattering is strongly enhanced, depending on size and refractive index (Figure 5a). This is expressed by the Mie efficiency factor, which is the ratio of the scattering cross-section σ_{scat} and the cross-sectional area of the beads along the long axis $A_l = \pi w_b l_b/4$. For spheroids consisting of chitin (Figure 5b), the efficiency factor has a maximum at short wavelengths. For beads with the measured refractive indices (Figure 5c), the scattering of visible light is strongly enhanced, with a pronounced maximum in the visible wavelength range. This is particularly pronounced outside the absorption wavelength range of the pterin pigments and leads to dramatic increases in the scattering cross-section of up to a factor of 14 (Figure S4, Supporting Information). The Mie modeling elucidates that the higher refractive index indeed causes a strong increase in scattering (Figure 5b,c). Furthermore, it shows that the shape of the spheroids is in fact optimized for light scattering in the visible wavelength range (Figures S5 and S6, Supporting Information).

3. Discussion

Through their incorporation into pierid wing scales, a granular medium with a high density of pigments produces high reflection. Concentration of the different pterin pigments in the spheroidal beads leads to an increased absorption coefficient of the beads in the short-wavelength range, which causes an increase in refractive index in the long-wavelength range. This results in very low scattering at short wavelengths and a much enhanced scattering at long wavelengths, thus creating a strong spectral contrast, giving rise to the strikingly vivid coloration of pierid butterflies. The wing brightness is further enhanced by the stacking of multiple scales.[28]

3.1. Refractive Index of Pterin-Containing Beads

What is the origin of the extremely high refractive indices of the pierid scale beads? Consider the example of a scale of *P. rapae* with a 400 nm thick bead layer (Figure 2d) and a peak absorbance of $D = 0.8$ (Figure S2, Supporting Information). This implies an extinction coefficient $\alpha = D/l_b = 2 \times 10^4$ cm^{-1}. Using a peak molar extinction coefficient of pterin $\varepsilon = 6 \times 10^3$ M^{-1} cm^{-1},[29] the concentration is $c = \alpha/\varepsilon = 3.3$ M, implying a volume per molecule of 5.5×10^{-24} l = 5.5 nm^3. As the volume filling factor of the granules in the bead layer is ≈0.3 (i.e., $f_V = 2f_A/3$; Table 1), the volume per pterin molecule in the beads is ≈1.7 nm^3, i.e., a cube with side length ≈1.2 nm. Although this volume is distinctly larger than a pterin molecule, it means that assembly of the pterin molecules in the beads approaches close packing.

3.2. Pigments in Biological Photonic Structures

Some open biological questions remain. In butterflies, the observed optical mechanism of ellipsoidal granular scatterers with high refractive index appears to have evolved uniquely in pierid butterflies. This may be related to the selection of pterins as coloring pigment. Other butterfly families employ ommochromes and kynurine (Nymphalidae[30]) or papiliochromes (Papilionidae[31]). Since these pigments are not concentrated in granules, their contribution to the refractive index may be minor. Yet, in all cases of animal coloration, the refractive index of the colored tissue plays a central role in creating vivid colors, specifically in the extremely thin tissues of insect wings, butterfly wing scales, and bird feather barbules. The melanosomes of bird plumage are another case of strongly pigmented nanosized particles.[32–35] The high refractive index of concentrated melanin pigment creates a refractive index contrast with the surrounding keratin matrix, which has a refractive index comparable to that of chitin.[18] In the bird feathers, the rod-like melanosomes are often arranged in periodic arrays, e.g., multilayers (e.g., bird-of-paradise[32]) or square-like matrices (e.g., peacock[34]). Light scattering from individual rodlets then becomes irrelevant and is replaced by strong photonic effects caused by light interference.

4. Conclusion

In conclusion, we have shown that quantitative knowledge of the refractive index is key to understanding the high reflection of pierid wing scales. Using Jamin–Lebedeff interference microscopy, we measured the refractive index of the highly pigmented beads across the visible wavelength range. The shape of the beads is presumably optimized for optimal scattering of visible light in the wavelength range where light absorption by the pigment is negligible.

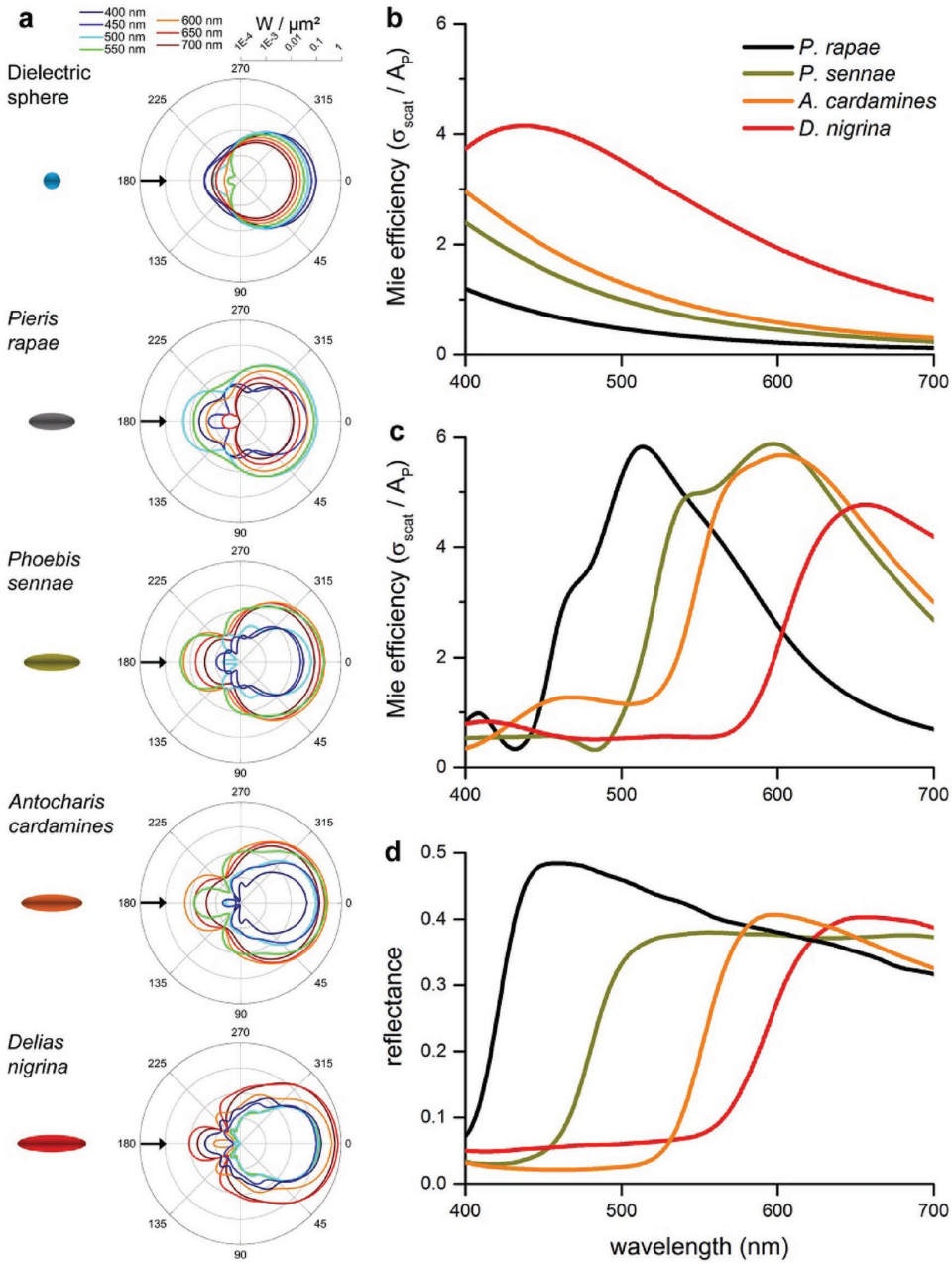

Figure 5. Mie scattering and single scale reflectance spectra. a) Angular scattering profiles for the different-sized spheroids and the measured refractive index profile of Figure 4 for wavelengths from 400 to 700 nm in 50 nm steps and unpolarized light. 0° implies forward-scattering (i.e., in the direction of light incidence) and 180° implies back-scattering (i.e., reflection toward the light source; Figures S7–S10 (Supporting Information) present the polarization-dependent profiles). b) Mie efficiency of dielectric spheroids consisting of chitin. c) Mie efficiency of spheroids having the measured refractive index dispersion. The Mie efficiency is dramatically increased due to the difference in refractive index. d) Reflectance spectra measured with a microspectrophotometer from single, isolated scales.

The discovered biological photonic properties are as yet to be reproduced artificially. The fact that tiny wing scales with thicknesses on the order of ≈500 nm reflect light very efficiently is rather surprising and should inspire material scientists,[36] e.g., by creating densely pigmented beads and arranging them irregularly on a surface.[37,38] This way, novel paints or thin, opaque paper may be produced as well as projection screens with large viewing angles.

5. Experimental Section

Specimens: The investigated specimens of the Small White, *Pieris rapae* (Linneaus, 1758) and the Orange Tip, *Anthocharis cardamines* (Linneaus, 1758), were caught locally around Groningen, the Netherlands. Specimens of the Cloudless Sulphur, *Phoebis sennae* (Linneaus, 1758) were purchased (www.insectsale.com), and Common Jezebel, *Delias nigrina* (Fabricius, 1775), were captured near Bateman's Bay (NSW, Australia). The photographs of Figure 1a–c were taken in

Naturalis (Natural History Museum, Leiden, the Netherlands); the specimen of Figure 1d was provided by Dr. M. F. Braby, Australian National University, Canberra.

Scanning electrom microscopy (SEM): The ultrastructure of the wing scales was investigated with a XL30-ESEM electron microscope (Philips, Eindhoven, the Netherlands) and a MIRA 3 LMH field-emission electron microscope (Tescan, Brno, Czech Republic). To prevent charging, the samples were sputtered-coated by a thin layer of palladium or gold prior to imaging.

Spectrophotometry: Reflectance spectra of the wings of intact butterflies were measured (in air) with a bifurcated fiber-optic probe. The probe comprised six light guides, delivering light from a halogen-deuterium source (spectral range: 250–1000 nm; AvaLight-D(H)-S; Avantes, Eerbeek, the Netherlands), which surrounded a central fiber that acted as collector of the reflected light (of a spot with diameter ≈1 mm, delivering it to a fiber optic spectrometer (spectral range 250–1000 nm; AvaSpec-2048; Avantes). A white diffusive reflectance standard (WS-2; Avantes) served as the reference. Absorbance spectra of single wing scales immersed in a refractive index matching fluid were measured with a custom-built microspectrophotometer (MSP). The light beam of a xenon light source was coupled with a quartz lens into the microscope, equipped with an Olympus 20×/0.45 objective. The spectral range of the MSP was limited to wavelengths ≥360 nm.

Kramers–Kronig Calculations: The refractive index of a medium is a wavelength-dependent complex number, with real part $n_R(\lambda)$ and imaginary part $n_I(\lambda)$; λ is the light wavelength. $n_I(\lambda)$ of a medium is related to the absorption coefficient $\kappa(\lambda)$ by $n_I(\lambda) = \lambda\kappa(\lambda)/(4\pi)$. For a homogeneous pigmented medium with thickness d, the absorption coefficient is obtained from the transmittance $T(\lambda)$, and absorbance $D(\lambda)$ spectra via

$$\kappa(\lambda) = -\ln[T(\lambda)]/d = 2.3D(\lambda)/d \quad (1)$$

The absorbance spectrum is generally measured only in a restricted wavelength range, yielding a wavelength-restricted $\kappa(\lambda)$. The resulting contribution of the pigment to the real part of the refractive index $n_R(\lambda)$ then is given by the Kramers–Kronig relation[6,22,23]

$$\Delta n_R(\lambda) = \frac{1}{2\pi^2}\int_0^\infty \frac{\kappa(\lambda')}{\left[1-(\lambda'/\lambda)^2\right]} d\lambda' \quad (2)$$

Jamin–Lebedeff Interference Microscopy: The real part of the refractive index of the butterflies' scales was measured by Jamin–Lebedeff polarizing interference microscopy. Scales were isolated by gently pressing the wings to a microscope slide, which was then submersed in a fluid with refractive index varying between 1.56 and 1.70 (series A or B of Cargille Labs, Cedar Grove, NJ, US), and subsequently covered by a cover slip. For each immersion fluid, the value of the refractive index as a function of the wavelength was derived from the refractive index value given for the wavelength 586 nm and its Abbe number, by using the Cauchy equation $n(\lambda) = A + B/\lambda^2$ and calculating the parameters A and B.[6,18] The microscope slide with immersed scales was mounted on the stage of a Zeiss Universal Microscope, set up for Jamin–Lebedeff interference microscopy. The microscope objective was a Zeiss Pol-Int I 10×/0.22. The light source was a xenon lamp connected to a motorized monochromator (PTI DeltaRam; Photon Technology International), yielding monochromatic light in the wavelength range 380–800 nm, with minimal step size of ≈5 nm. At each wavelength, the angular position of the analyzer was changed in steps of 10°, and after each step a photograph was taken with a Coolsnap ES monochrome camera (Photometrics, Tucson, AZ). The resulting image stack was subsequently evaluated with Python scripts (www.python.org) that determined the phase changes of the local sinusoidal intensity profiles, from which the refractive index was derived with the procedure as described before.[6,21]

Light Scattering of 3D Particles: The light scattering of differently sized spheroids was simulated with 3D finite-difference time-domain (FDTD) calculations. Lumerical FDTD Solutions 8.15 was used, a commercial-grade Maxwell equation solver. Each particle was placed in a simulation volume of $2 \times 2 \times 2$ μm^3 and surrounded by a total-field scattered-field source. Different analysis groups, each consisting of various power monitors were used: one in the total field region (inside the light source) and one in the scattered field region (outside the light source). With these analysis groups, the scattering cross-section, σ_{scat}, as well as the angular distribution of scattered radiation could be extracted. The light source covered a wavelength range from 400 to 700 nm. For the particles, different refractive indices were tested using either the measured refractive index dispersion profile from the Jamin–Lebedeff measurements (Figure 4) or published data for chitin using $n(\lambda) = 1.517 + 8800/\lambda^2$.[18]

Supporting Information

Supporting Information is available from the Wiley Online Library or from the author.

Acknowledgements

The authors thank Dr. Wesley Browne, Dr. Gerd Schröder-Turk, and Dr. Silvia Vignolini for stimulating discussions and comments on an early version of the manuscript and James A. Dolan and Karl C. Gödel for technical assistance. This research was partly supported through the National Centre of Competence in Research "Bio-Inspired Materials" and the Adolphe Merkle Foundation (to B.D.W. and U.S.), the Ambizione program of the Swiss National Science Foundation (PZ00P2_168223, to B.D.W.), and the Air Force Office of Scientific Research/European Office of Aerospace Research and Development AFOSR/EOARD (Grant FA9550-15-1-0068, to D.G.S.).

Received: October 23, 2016
Published online: November 28, 2016

[1] L. P. Biró, J. Vigneron, *Laser Photonics Rev.* **2011**, *5*, 27.
[2] J. D. Joannopoulos, *Photonic Crystals: Molding the Flow of Light*, 2nd ed., Princeton University Press, Princeton, NJ **2008**.
[3] M. Müller, R. Zentel, T. Maka, S. G. Romanov, S. Torres, *Adv. Mater.* **2000**, *12*, 1499.
[4] B. P. Cumming, M. D. Turner, G. E. Schröder-Turk, S. Debbarma, B. Luther-Davies, M. Gu, *Opt. Express* **2014**, *22*, 689.
[5] M. Srinivasarao, *Chem. Rev.* **1999**, *99*, 1935.
[6] D. G. Stavenga, H. L. Leertouwer, B. D. Wilts, *Light: Sci. Appl.* **2013**, *2*, e100.
[7] T. M. Trzeciak, B. D. Wilts, D. G. Stavenga, P. Vukusic, *Opt. Express* **2012**, *20*, 8877.
[8] B. D. Wilts, A. Matsushita, K. Arikawa, D. G. Stavenga, *J. R. Soc. Interface* **2015**, *12*, 20150717.
[9] H. Ghiradella, *Microsc. Res. Tech.* **1994**, *27*, 429.
[10] H. Ghiradella, *Adv. Insect Physiol.* **2010**, *38*, 135.
[11] D. G. Stavenga, S. Stowe, K. Siebke, J. Zeil, K. Arikawa, *Proc. R. Soc. B* **2004**, *271*, 1577.
[12] B. Wijnen, H. L. Leertouwer, D. G. Stavenga, *J. Insect Physiol.* **2007**, *53*, 1206.
[13] K. Arikawa, M. Wakakuwa, X. Qiu, M. Kurasawa, D. G. Stavenga, *J. Neurosci.* **2005**, *25*, 5935.
[14] N. I. Morehouse, P. Vukusic, R. Rutowski, *Proc. R. Soc. B* **2007**, *274*, 359.
[15] R. O. Prum, J. A. Cole, R. H. Torres, *J. Exp. Biol.* **2004**, *207*, 3999.
[16] L. M. Mäthger, E. J. Denton, N. J. Marshall, R. T. Hanlon, *J. R. Soc. Interface* **2009**, *6*, S149.

[17] L. M. Mäthger, S. L. Senft, M. Gao, S. Karaveli, G. R. Bell, R. Zia, A. M. Kuzirian, P. B. Dennis, W. J. Crookes-Goodson, R. R. Naik, *Adv. Funct. Mater.* **2013**, *23*, 3980.
[18] H. L. Leertouwer, B. D. Wilts, D. G. Stavenga, *Opt. Express* **2011**, *19*, 24061.
[19] S. Yoshioka, S. Kinoshita, *Phys. Rev. E* **2011**, *83*, 051917.
[20] R. L. Rutowski, J. M. Macedonia, N. Morehouse, L. Taylor-Taft, *Proc. R. Soc. B* **2005**, *272*, 2329.
[21] D. G. Stavenga, H. L. Leertouwer, D. C. Osorio, B. D. Wilts, *Light: Sci. Appl.* **2015**, *4*, e243.
[22] V. Lucarini, J. J. Saarinen, K. Peiponen, E. M. Vartiainen, *Kramers-Kronig Relations in Optical Materials Research*, Vol. *110*, Springer Science & Business Media, Berlin, Germany **2005**.
[23] H. M. Nussenzveig, *Causality and Dispersion Relations*, Academic Press, New York, USA **1972**.
[24] D. A. G. Bruggeman, *Ann. Phys.* **1935**, *24*, 636.
[25] J. A. Stratton, *Electromagnetic Theory*, John Wiley & Sons, Hoboken, NJ, USA **2007**.
[26] I. S. Saidi, S. L. Jacques, F. K. Tittel, *Appl. Opt.* **1995**, *34*, 7410.
[27] E. J. McCartney, *Optics of the Atmosphere: Scattering by Molecules and Particles*, Wiley, New York **1976**.
[28] D. G. Stavenga, M. A. Giraldo, B. J. Hoenders, *Opt. Express* **2006**, *14*, 4880.
[29] P. J. Van Haastert, R. J. De Wit, Y. Grijpma, T. M. Konijn, *Proc. Natl. Acad. Sci. USA* **1982**, *79*, 6270.
[30] D. G. Stavenga, H. L. Leertouwer, B. D. Wilts, *J. Exp. Biol.* **2014**, *217*, 2171.
[31] Y. Umebachi, *Zool. Sci.* **1985**, *2*, 163.
[32] B. D. Wilts, K. Michielsen, H. De Raedt, D. G. Stavenga, *Proc. Natl. Acad. Sci. USA* **2014**, *111*, 4363.
[33] H. Durrer, *Denkschr. Schweiz. Naturforsch. Ges.* **1977**, *91*, 1.
[34] J. Zi, X. Yu, Y. Li, X. Hu, C. Xu, X. Wang, X. Liu, R. Fu, *Proc. Natl. Acad. Sci. USA* **2003**, *100*, 12576.
[35] R. Maia, R. H. F. Macedo, M. D. Shawkey, *J. R. Soc. Interface* **2012**, *9*, 734.
[36] C. Sanchez, H. Arribart, M. M. Guille, *Nat. Mater.* **2005**, *4*, 277.
[37] Y. Takeoka, S. Yoshioka, A. Takano, S. Arai, K. Nueangnoraj, H. Nishihara, M. Teshima, Y. Ohtsuka, T. Seki, *Angew. Chem. Int. Ed.* **2013**, *52*, 7261.
[38] M. Xiao, Y. Li, M. C. Allen, D. D. Deheyn, X. Yue, J. Zhao, N. C. Gianneschi, M. D. Shawkey, A. Dhinojwala, *ACS Nano* **2015**, *9*, 5454.